

Failure Analysis of Oil Tubes Containing Corrosion Defects Based on Finite Element Method

Xiaoben Liu^{1,*}, Hong Zhang^{1,2,*}, Meng Li¹, Qinquan Duan¹, Yanfei Chen¹

¹ College of Mechanical and Transportation Engineering, China University of Petroleum, Beijing, 102249, China

² China University of Petroleum(Beijing) Karamay Campus, Karamay, 834000, China

*E-mail: liuxiaoben1991@126.com; HZhang@cup.edu.cn

Received: 31 October 2015 / *Accepted:* 30 March 2016 / *Published:* 4 May 2016

Oil tubes containing corrosion defects are vulnerable under complicated service load. In the oil field, corrosion of oil tubes is mainly electrochemical corrosion. In this study, failure analysis of the oil tube with two typical electrochemical corrosion defects, the grooving defect and the ellipsoidal pit, was conducted by finite element method. The complicated service load conditions were considered, and the effects of the defect dimensions on the strength of the tube were discussed in detail. Results show that, with the increase of the depth of the defect position in the tube for both defect types, the peak Mises stress decreases first and then increases. If the defect is in the shallow position of the tube, it is the axial tension that leads to the tensile fracture. But if the defect is in the deep position of the tube, it is the internal pressure that leads to the rupture. The depth of the defect has great influence on the tube strength, while the width and length of the defect have small influence on the tube strength, especially when the defect is in the shallow position of the tube. This study can be referenced for the failure analysis and strength evaluation of oil tubes with corrosion defects.

Keywords: N80 oil tube, electrochemical corrosion defects, complicated service load, finite element method, failure analysis

1. INTRODUCTION

The oil tube is one of critical structures in the oil and gas industry with complex working condition, which demands huge consumption. It is of great significance to conduct a study on the failure behavior of the oil tube under complicated working conditions for the safety of oil and gas production. As one of three failure types, the corrosion in the petroleum industry led to 6% of the loss of the entire industry. The main corrosion environment is the corrosive electrolyte solution using

water as solvent, which is also highly mineralized solution with various ions, so the corrosion of oil tubes is mainly electrochemical corrosion with high rate. At the anode area, iron is resolved into iron ion, then into electrolyte. Then the corrosion cell is formed, and REDOX reaction is performed. Lots of investigation have been conducted for electrochemical corrosion behavior of tubing steels in recent years. Li [1] studied the joint effect of temperature, stress states and sulfur ions on the electrochemical corrosion behavior of N80 tubing steel. Xue [2] employed potentiodynamic polarization measurement and electrochemical impedance spectroscopy to investigate the corrosion behavior of CT80 coiled tubing steel in artificial high salinity brine corresponding to the oil well water at Changqing oil field. The same methods were also adopted by Ren [3] to study the effects of temperature of electrochemical corrosion behavior of the CT80 steel. Liu [4] studied the effect of solution pH value and H₂S partial pressure on the electrochemical corrosion of P110 tubing steel in solutions containing dissolved H₂S/CO₂ in an autoclave.

When electrochemical corrosion occurs in the oil tube, induced corrosion defects will reduce the strength of the tube seriously. Large concentrated stress will be induced in the corrosion areas, when corroded oil tubes are subjected to combined working loads, leading to rupture failure as shown in Fig. 1. Hence the failure analysis on the oil tube containing corrosion defects under complicated working loads is of practical value for ensuring the safety of oil tubes.



a) Tube fracture induced by corrosion b) Corrosion perforation in the tube

Figure 1. Oil tubes containing corrosion defects

Intensive research work has been conducted on failure analysis and corresponding assessment method for corroded pipe structures. Two typical kinds of methods were commonly used, the standard based evaluation and the finite element method based numerical analysis. The standard based evaluation methods are suitable for corroded onshore and offshore pipelines, for a series of standards have been established for failure assessment of corroded pipelines, e.g. ASME B31G [5], API 579 [6], DNV RP101 [7]. While none standards suitable for assessment of corroded oil tubes has been proposed, most researchers conducted numerical analysis for strength analysis of corroded oil tubes. Zhou [8] discussed the failure criteria of oil tubes with corrosion defects, based on nonlinear finite element model. Zhang [9] conducted finite element analysis on the oil tube containing spherical corrosion pit under pure bending effect. Hu [10] conducted reliability analysis of marine risers with

narrow and long corrosion defects under combined load. Xia [11] derived the influence of the corrosion defect dimensions on the oil tube by parametric analysis using finite element models. Shi [12] conducted numerical and experimental study on the effects of the corrosion defect volume on the resistance of the tube to internal pressure. And similar numerical analysis studies were also conducted on corroded pipelines. Fu [13] studied the failure pressure of internally corroded line pipe by finite element method. Batte [14] proposed a method for determining the residual strength of corroded pipelines. Based on damage theory, Choi [15] developed a limit pressure prediction model for corroded X65 steel. Zhu [16] first considered the influence of the hardening behavior of the pipe steel on the pipe limit pressure. Cronin [17] investigated the failure pressure of low strength corroded pipeline numerically and experimentally. Chen [18] predicted the failure pressure for pipeline with two corrosion defects using nonlinear finite element analysis. Ma [19] proposed a regression formula for high strength pipeline limit pressure, and Chen [20] improved this work by studying the effects of the multi corrosion defects on the failure analysis of high strength pipelines. Zhang [21] investigated the failure pressures of corrosion pipeline with single and multi point ellipsoidal corrosion defects, considering effects of various factors.

Although their contributions made are significant, less attention is paid on the effects of the complicated load conditions on the strength and failure modes of corroded oil tubes in service, which is very important in the engineering practice. To fill this gap, failure analysis of oil tubes with corrosion defects under different combined service loads was conducted systematically in this study. The common defect types were considered, including the ellipsoidal pit and grooving defect. The influence of the loading conditions and defect dimensions on the tube strength was discussed in detail, and the failure mode of the tube was also investigated for all conditions. This study can be referenced for the safety evaluation of oil tubes with corrosion defects.

2. BASIC THEORY ANALYSIS

2.1. Stress analysis of the oil tube under working conditions

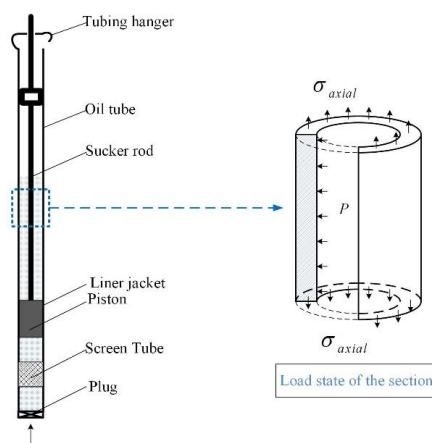


Figure 2. The stress state of the oil tube in working conditions

The working condition of the oil tube is complicated. Normally, it is under axial tension due to gravity and other loads, along with hoop tension due to internal pressure. And in some special cases, such as the case where the tubing is in a curved well, it can also be under bending, which makes the stress state more complicated. In this study, the axial stress and the internal pressure were considered in detail, while the bending stress was ignored. Fig. 2 illustrates the stress state of the oil tube in working conditions. The axial stress and internal pressure vary with the depth of position in the oil tube.

2.2. Axial Stress

The axial force F in the oil tube is complicated. It comprises the gravity force of the tube F_1 , the buoyancy of the liquid in the well F_2 , the liquid force F_3 , the friction force between the piston and bushing F_4 , the friction force between the pumping rod and the oil tube F_5 and so on [8]. Fig. 3 plots the load spectrum of the axial force in the oil tube [22]. It can be shown that the axial force peaks in the down stroke, and at this moment the axial force can be calculated as follows:

$$F = F_1 - F_2 + (F_3 + F_4 + F_5) \quad (1)$$

And the axial stress σ_{axial} can be easily obtained as:

$$\sigma_{axial} = F / A \quad (2)$$

Where, A is the section area of the oil tube, mm^2 .

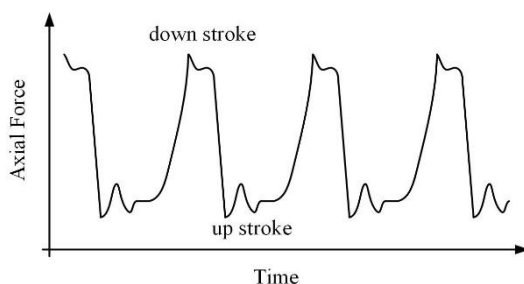


Figure 3. Load spectrum of the axial force in the oil tube

2.3. Internal Pressure

The internal pressure can be derived by the following formula:

$$P = \rho_0 gh + \sigma_0 \quad (3)$$

Where, ρ_0 is the density of the oil in the tube, kg/m^3 . g is the acceleration of gravity, m/s^2 . h is the depth of the position in the oil tube, m . σ_0 is the oil pressure in the well head, MPa .

2.4. Failure criteria of the oil tube

The tube steel is elastic-plastic and isotropic material, which has good comprehensive mechanical properties (i.e. strength, plasticity and toughness). The main damage form of the oil tube

with corrosion defects is local plastic failure. According to ISO/TR 10400:2007 [23], it can be considered that the failure occurs in the tube, when peak Von Mises stress in the corrosion area σ_e reaches the flow stress σ_f , which can be calculated by the following equations.

$$\sigma_f = (\sigma_s + \sigma_b) / 2 \quad (4)$$

Where, σ_s is the yield strength, MPa. σ_b is the tensile strength, MPa.

$$\sigma_e = \sqrt{\frac{1}{2} [(\sigma_1 - \sigma_2)^2 + (\sigma_1 - \sigma_3)^2 + (\sigma_2 - \sigma_3)^2]} \quad (5)$$

Where, σ_1 , σ_2 , σ_3 are the three principal stresses, MPa.

3. NUMERICAL MODELING

3.1. Basic assumptions

- a) The oil tube is assumed to be with no initial defect.
- b) The tube steel is elastic-plastic and isotopic.
- c) Fracture failure occurs in the tube, when the equivalent stress reaches the flow stress.

3.2. Material properties

The N80 steel widely used in the oil field in China was selected in this study. The multi linear isotropic hardening model was used to simulate the steel material in the numerical model. The stress-strain curve of the N80 steel is shown in Fig. 4. The elastic modulus E is 207GPa, the yield strength σ_s is 550MPa, the tensile strength σ_b is 690MPa, the flow stress σ_f is 620 MPa, and the Poisson ratio ν is 0.3 [24].

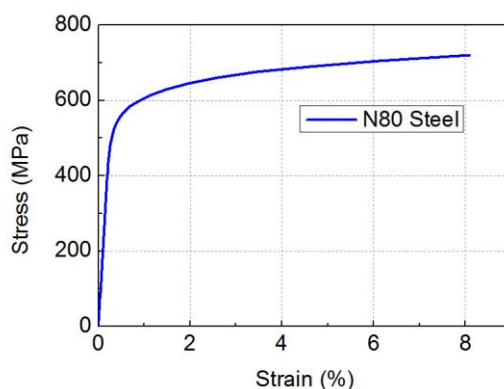


Figure 4. Stress-strain relationship for the N80 steel

3.3. Finite element model

The corrosion defect in the tube can be defined by three parameters, the depth of the defect d , mm, the length of the defect L , mm, the width of the defect W , mm, as shown in Fig. 5. As the corrosion defect is small compared with the whole tube, when establishing the finite element model, only a small part is needed to be considered. Therefore, the axial stress in the model can be considered as a constant. According to the Saint-Venant's Principle, in order to avoid the influence of the boundary conditions, the axial length of the oil tube is set to be four times of the tube's diameter.

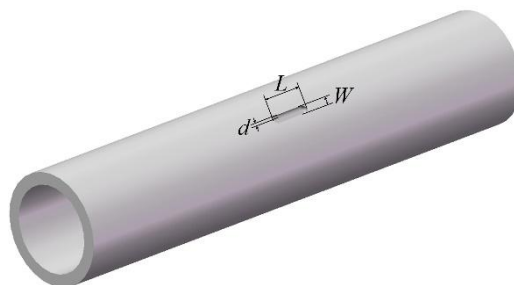


Figure 5. The defect parameters schemes of the oil tube

Based on the symmetry of the load condition and the geometric model, only 1/4 of the oil tube part was built in the finite element modeling. Two typical corrosion defect types were considered in this study, the grooving defect and the ellipsoidal pit, as shown in Fig. 6. The general finite element software ANSYS was adopted in this study to conduct the finite element analysis [25]. The 8-node hexahedral element SOLID186 was used to simulate the oil tube. A fine mesh was employed for the defect area, where the maximum stress and strain are expected, while a coarser mesh was chosen for the other parts. As the wall of oil tube is generally thick, it was discretized into 4 equal sized 8-node hexahedral elements in the radial direction, which makes the result more accurate. Fig.6 depicts the meshed model. In this figure, the meshing details of the two kinds of defects were given respectively.

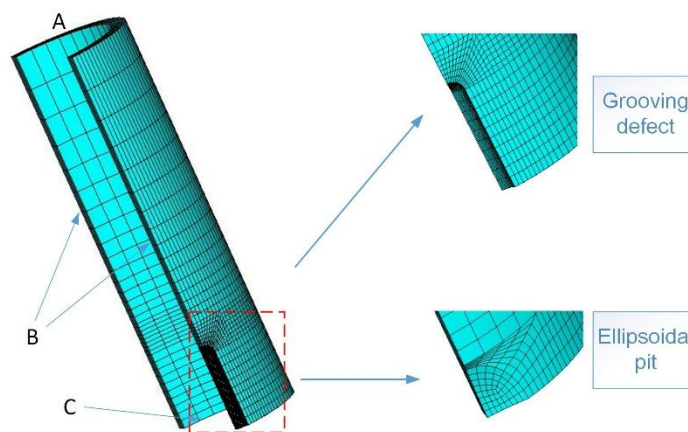


Figure 6. Finite element model of one fourth oil tube with corrosion defect

As shown in Fig.6, the left side of the tube (plane B in Fig. 6) and the downside of the tube (plane C in Fig. 6) are the symmetrical planes in the quarter model, where the symmetric boundary conditions were applied. To simulate the effect of the axial load, tensile axial stress was applied to the top side of the tube (plane A in Fig. 6). And the internal pressure was applied to the inside surface of the tube to simulate the effect of the liquid pressure on the tube.

4. RESULTS AND DISCUSSION

4.1. Load conditions

In this study, parameters of a 4000-meter-deep oil well were selected for the analysis. The size of the N80 steel oil tube is as follows, the diameter $D=88.9\text{mm}$, and the wall thickness $t=7.34\text{mm}$. The other parameters of the oil well are listed in Table 1.

Based on the values above and Eqs. 1-3, the distribution of the axial stress and the internal pressure in the tube can be obtained, as shown in Fig. 7. It is obvious that, with the increase of the depth h , the internal pressure increases linearly, while the axial stress decreases linearly.

Table 1. Basic parameters for the oil well

Item	Value
Pump depth (m)	4000
Liquid level depth (m)	3500
oil density (kg/m^3)	973
fluid viscosity (Pa.s)	0.025
Wellhead pressure (MPa)	6

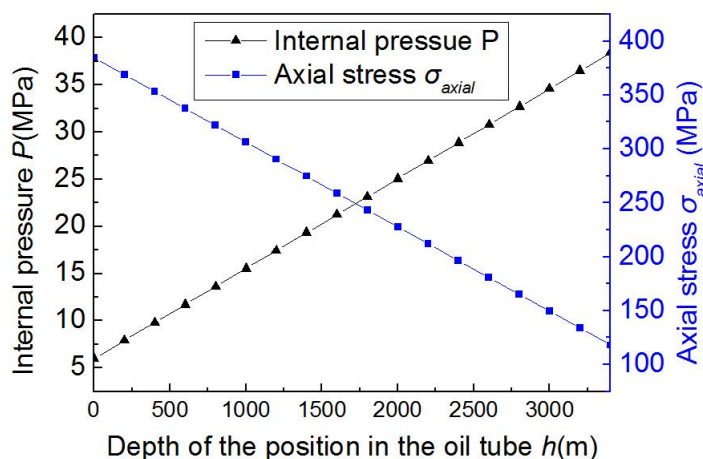


Figure 7. Distribution of the axial stress and internal pressure in the tube

4.2. Effects of the load conditions

The corrosion defects at various depth position in the tube was discussed here to study the failure mode of the tube under different load conditions. Two sizes of the corrosion defect were considered here. The size of the grooving defect is $d=4\text{mm}$, $W=18\text{mm}$, $L=60\text{mm}$. The size of the ellipsoidal pit is $d=4\text{mm}$, $W=18\text{mm}$, $L=26\text{mm}$.

Fig. 8 illustrates the change law of the peak Von Mises stress in the corrosion area σ_e with the depth of the defect in the tube h . It can be obtained that for both kinds of defect, with the increase of h , σ_e decreases first and then increases. When the depth of the defect position in the tube h is less than 1600m, the peak Von Mises stress σ_e of the ellipsoidal pit is larger than that of the grooving defect. When h is larger than 1600m, σ_e of the ellipsoidal pit is smaller than that of the grooving defect. So it can be derived that, with the same other dimensions of the defect, the tube containing the ellipsoidal pit is more vulnerable when the defect is in the shallow position of the tube, while the tube containing the grooving defect is more vulnerable when the defect is in the deep position of the tube.

If the peak Von Mises stress in the corrosion area σ_e reaches the flow stress σ_f of the N80 steel, the failure will occur in the tube. Point A and B refer to the failure positions of the ellipsoidal pit and the grooving defect, respectively. For the cases considered here, the failure will appear in the ellipsoidal pit when $h < 600\text{m}$. In this case, the large Mises stress mainly induced by the axial stress in the tube is concentrated in the center line of the pit in the axial direction of the tube, as shown in the left stress contour in Fig.8, which may lead to tensile fracture failure. The failure will appear in the grooving defect when $h > 2200\text{m}$. In this case, the large Mises stress mainly induced by the internal pressure is concentrated in the center line of the defect in the circumferential direction leading to rupture failure, as shown in the right stress contour in Fig.8, which is a typical failure mode of corroded pipelines.

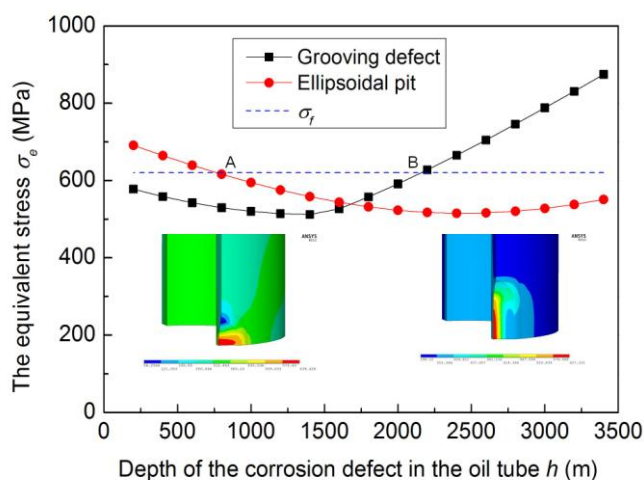


Figure 8. The trends of the Von Mises stress with the depth position of the defect

The Von Mises stress contours of both defects at various depth positions are listed in Fig. 9 in detail. Fig. 9(a) shows that, when h is small, the peak stress of the grooving defect concentrates at the top end of the defect. And with the increase of h , the stress concentration position moves to the center line of the defect in circumferential direction. Fig. 9(b) shows that, when h is small, the peak stress of the ellipsoidal pit concentrates in the center area of the pit in the axial direction. And with the increase of h , the concentration position moves to the center point of the pit.

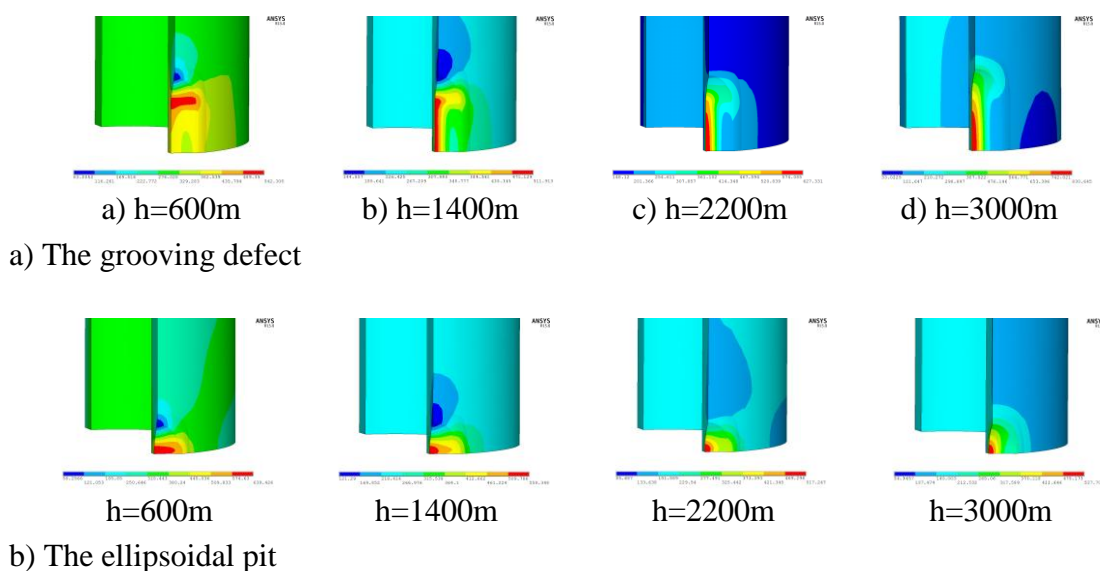


Figure 9. The Von Mises stress contours of the corrosion defect with various depth positions

4.3. Effects of the defect dimensions

4.3.1. Effect of the depth of the defect

The ratio of the depth of the defect to the tube wall thickness d/t was used here to study the effect of the depth of the defect on the tube strength. As derived above, the oil tube has various failure modes with different depths of the defect in the tube. Two typical load conditions were considered here for both corrosion types to study the influence of the depth of the defect on the tube strength.

Under condition I, the depth of the defect in the tube $h=400\text{m}$, which means the axial stress is 353.1 MPa, and the internal pressure is 9.8 MPa. Under condition II, the depth of the defect in the tube $h=3000\text{m}$, which means the axial stress is 196.3 MPa, and the internal pressure is 28.9 MPa. The length of the grooving defect is 60mm, and the length of the ellipsoidal pit is 26mm.

Fig. 10 illustrates the trends of the peak Von Mises stress σ_e with d/t under condition I, for the grooving defect and ellipsoidal pit, respectively. It can be shown that the depth of the defect has great influence on the tube strength, σ_e increases almost linearly with the increase of d/t for both defect types. And σ_e varies in a small range for different widths of the defect. For the grooving defect, if the width of the defect $W=10\text{mm}$, the failure occurs when $d/t=0.55$. And if $W=14$ and 18mm , the failure occurs when $d/t=0.65$. For the ellipsoidal pit, the failure occurs when d/t arounds 0.55.

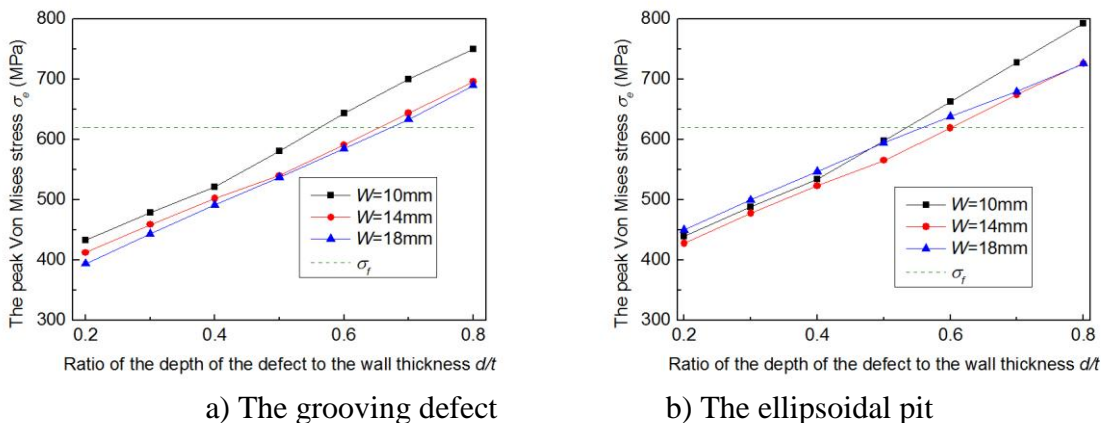


Figure 10. The trends of the peak Von Mises stress with the depth of the corrosion defect under load condition I

Fig.11 shows the Mises stress contours in the corrosion areas with $W=14\text{mm}$ for a series of defect depths under load condition I. For the grooving defect, the Mises stress concentrates at the top area of the defect, and with the increase of the depth of the defect, the stress concentration becomes more severe. For the ellipsoidal pit, when $d/t=0.2$, the Mises stress in the whole corrosion area is large, but with the increase of d/t , the peak Mises stress concentrates at the top end of the pit in axial direction.

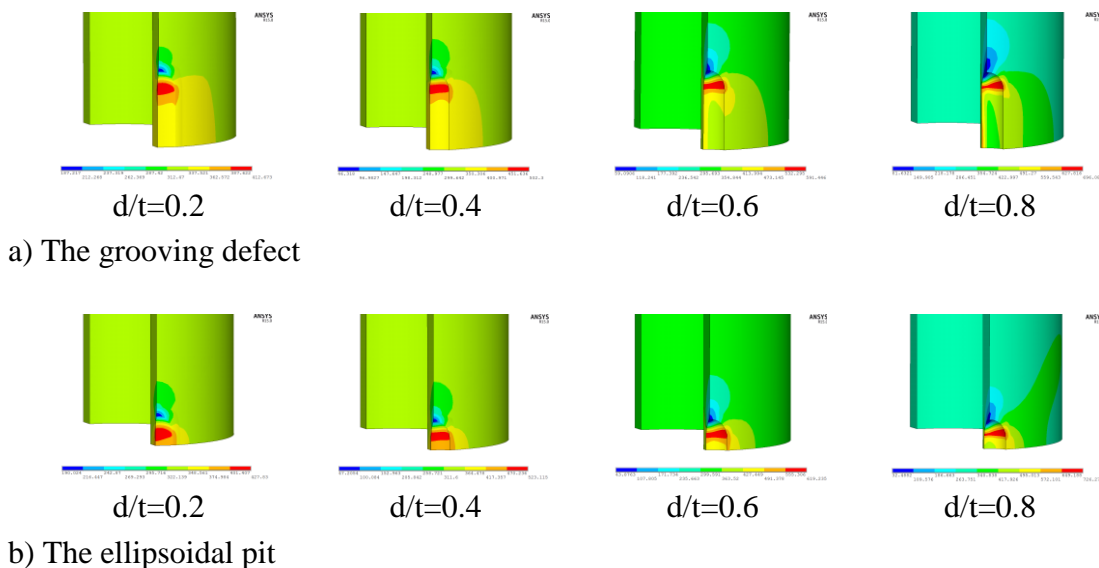


Figure 11. The Von Mises stress contours of the corrosion area with various d/t under load condition I

The stress behavior of the tube under load condition II differs from that under load condition I. Fig. 12 illustrates the trends of σ_e with d/t under condition II. σ_e increases with the increase of d/t for both defect types, and σ_e increases faster with a larger d/t , especially for the grooving defect. σ_e also varies in a small range for different widths of the defect. The trends of σ_e with d/t is in good

agreement with the results derived from corroded pipelines [19]. For the grooving defect, the failure occurs when d/t is larger than 0.45. And for the ellipsoidal pit, the failure occurs when d/t is larger than 0.6.

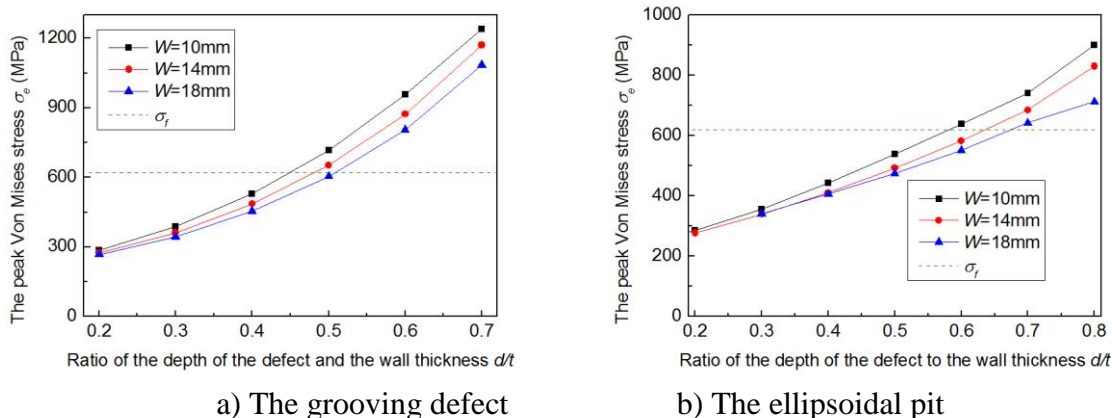


Figure 12. The trends of the peak Von Mises stress with the depth of the corrosion defect under load condition II

Fig.13 shows the Mises stress contours in the corrosion areas with $W=14\text{mm}$ for a series of defect depth under load condition II. It is obvious that the stress distribution for both defects are different with the one under condition I, as shown in Fig. 11. For both the grooving defect and the ellipsoidal pit, when $d/t=0.2$, the Mises stress in the whole center area is large. With increase of d/t , the Mises stress concentrates on the center line in the circumferential direction gradually.

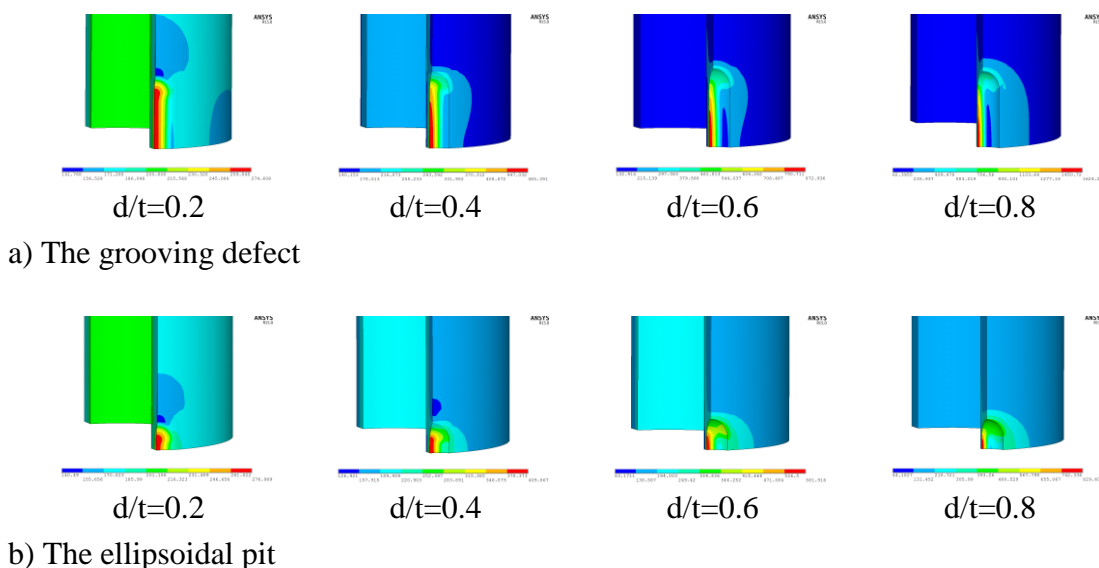


Figure 13. The Von Mises stress contours of the corrosion area with various d/t under load condition II

4.3.2. Effects of the width of the defect

The influence of the width of the defect on the tube strength was investigated in detail. Six widths i.e. 10mm, 12mm, 14mm, 16mm, 18mm, 20mm, were taken into consideration for both types of defect.

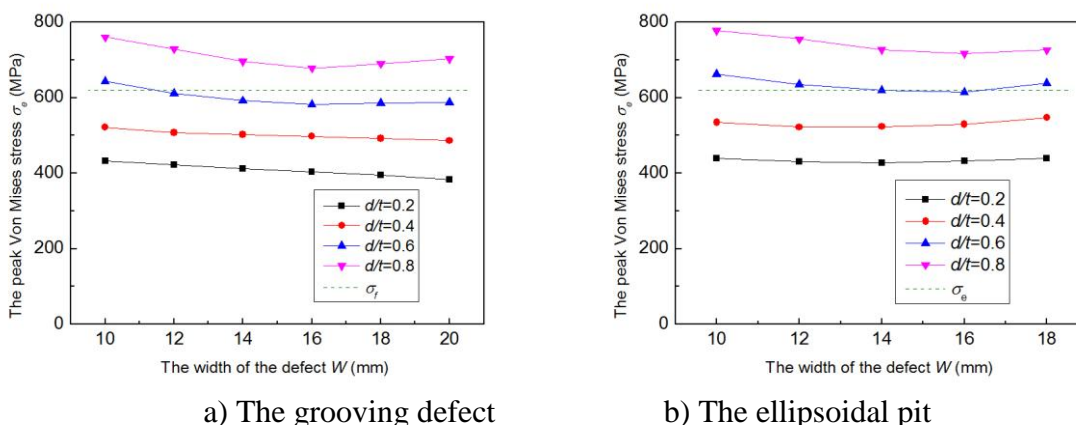


Figure 14. The trends of the peak Von Mises stress with the width of the corrosion defect under load condition I

Fig. 14 illustrates the trends of the peak Von Mises stress σ_e with the defect width W under condition I, for the grooving defect and ellipsoidal pit, respectively. It is obvious that, W has little influence on σ_e for both defect types. σ_e will only change about 40MPa, when W changes from 10mm to 20mm. Compared with the influence induced by the depth of the defect, the one induced by the width of the defect is quite small.

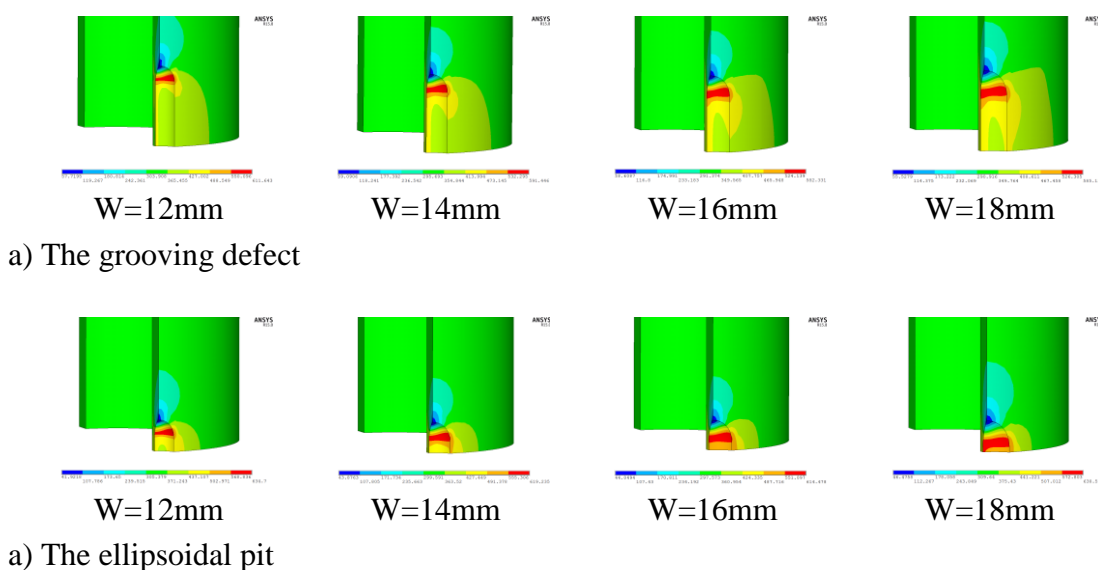


Figure 15. The Von Mises stress contours of the corrosion area with various W under load condition I

Fig.15 shows the Mises stress contours in the corrosion areas with $d/t=0.6$ for a series of defect depth under load condition I. For the grooving defect, the Mises stress concentrates at the top end of the defect, and with the decrease of the width of the defect, the stress concentration becomes more severe. For the ellipsoidal pit, if the width of the defect $W=18\text{mm}$, the Mises stress in the whole corrosion area is large. And with the decrease of W , the Mises stress concentrates at the top of the pit.

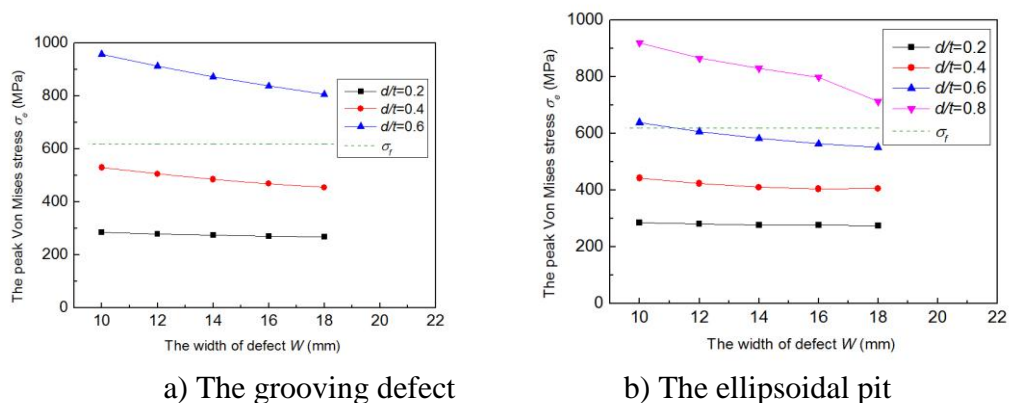


Figure 16. The trends of the peak Von Mises stress with the width of the corrosion defect under load condition II

Fig. 16 illustrates the trends of the peak Von Mises stress σ_e with the defect width W under load condition II. In this condition, σ_e decreases with the increase of W for all the cases. When $\sigma_e < \sigma_f$, the value of σ_e varies in a small range with the change of W .

Fig. 17 shows the Mises stress contours in the corrosion areas with $d/t=0.6$ for a series of defect depths under load condition II. For the grooving defect, the Mises stress concentrates on the center line of the defect in the circumferential direction. No obvious change occurs when W varies. For the ellipsoidal pit, the Mises stress concentrates on the center line of the pit in the circumferential direction when $W=12\text{mm}$. And with the increase of W , the Mises stress concentrates at the center point of the pit gradually.

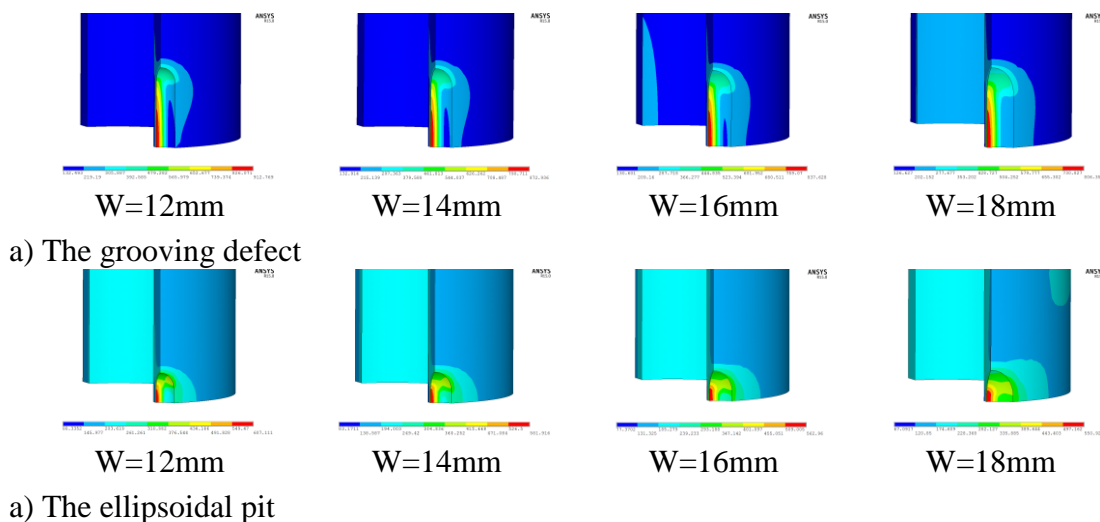


Figure 17. The Von Mises stress contours of the corrosion area with various W under load condition II

4.3.3. Effects of the length of the defect

Fig. 18 illustrates the relationship between the peak Von Mises stress σ_e and the length of the defect L , with different depths of the defect under load condition I. The width of the defect $W=16\text{mm}$ was selected for all cases in this section. Both defect types were considered by changing L in a large range. The defect is ellipsoidal pit if $L<35\text{mm}$, and is grooving defect if $L>35\text{mm}$. It can be obtained that, under load condition I, L has negligible influence on the tube strength, σ_e only decreases in a very small range when L increases from 26mm to 30mm, and σ_e is almost the same when L is larger than 40mm.

The Mises stress contours in the corrosion areas with $d/t=0.6$ for a series of the defect lengths under load condition I are shown in Fig. 19. It can be derived that, the length has no influence on the Mises stress distribution of the defect, the peak Mises stress concentrates at the end of the defect in the axial direction in all cases.

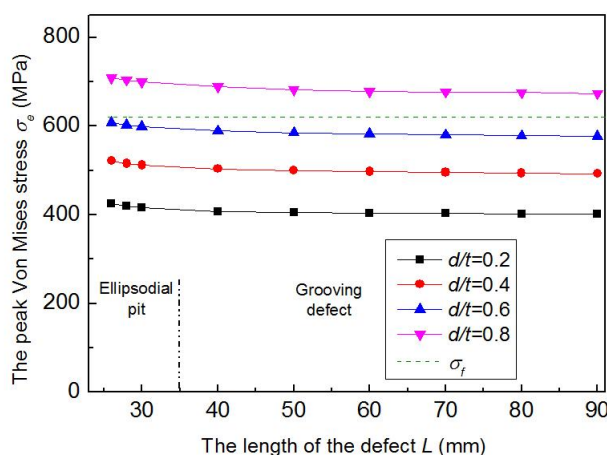


Figure 18. The trends of the peak Von Mises stress with the length of the corrosion defect under load condition I

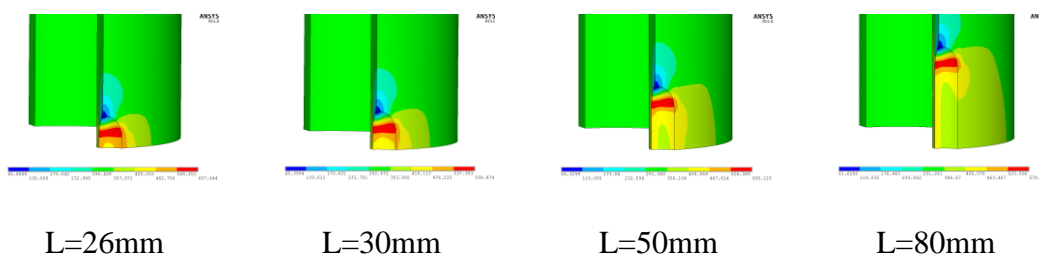


Figure 19. The Von Mises stress contours of the corrosion area with various L under load condition I

The relationship between the peak Von Mises stress σ_e and the length of the defect L under load condition II is shown in Fig. 20. If $d/t \leq 0.4$, σ_e is smaller than σ_f , none failure occurs in the tube. Under this circumstance, L has negligible influence on σ_e . The trends of σ_e with L is in good

agreement with the results derived from corroded pipelines [19]. If $d/t=0.6$, σ_e increases obviously with the increase of L . Under this circumstance, σ_e is larger than σ_r , if L is larger than 30mm.

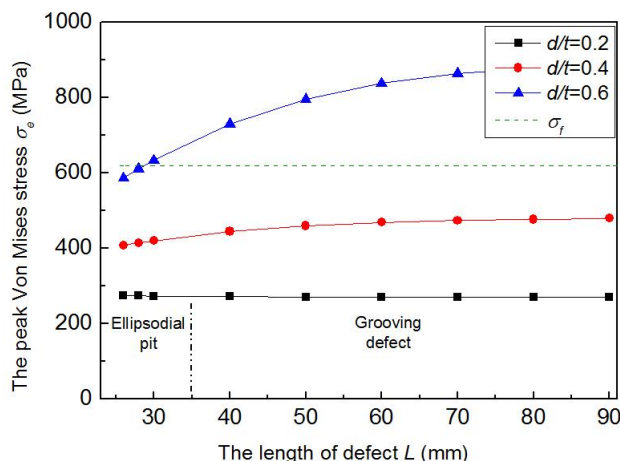


Figure 20. The trends of the peak Von Mises stress with the length of the corrosion defect under load condition II

Fig.21 shows the Mises stress contours in the corrosion areas with $d/t=0.6$ for a series of defect depths under load condition II. The Mises stress concentrates on the center line of the defect in the circumferential direction. With the increase of the length, the concentration area becomes larger.

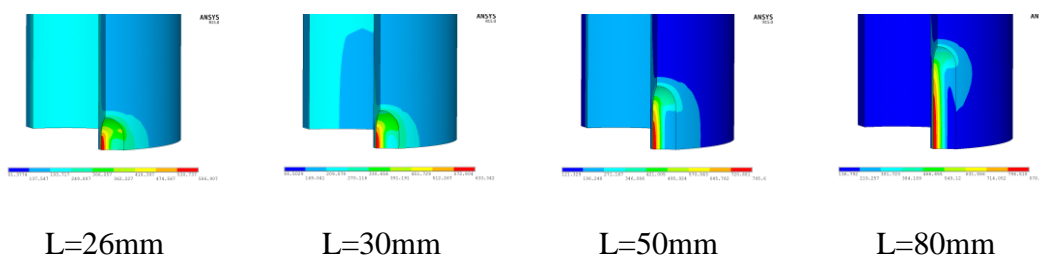


Figure 21. The Von Mises stress contours of the corrosion area with various L under load condition II

5. CONCLUSIONS

In this paper, a finite element model for failure analysis of N80 oil tube with corrosion defects was established by general finite element software ANSYS. The complicated working load conditions of the oil tube were taken into consideration. The influences of the defect dimensions on the tube strength and the failure mode of the tube were discussed in detail. Conclusions can be drawn as follows:

- (1) With the increase of the depth position of the defect in the tube, the peak Mises stress decreases first and then increases for both defect types.
- (2) If the defect is in the shallow position of the tube, the failure will occur due to axial

tension. The tube containing ellipsoidal pit will fracture in axial direction in the center of the pit, and the tube containing grooving defect will fracture in the axial direction at the end of defect. If the defect is in the deep position of the tube, the tube will rupture in the center line of the defect in the circumferential direction for both types of defects due to the internal pressure.

(3) The depth of the defect has great influence on the tube strength in all conditions. With the increase of the depth of the defect, the peak Mises stress increases in a large range, and the stress concentration becomes more severe.

(4) If the defect is in the shallow position of the tube, the width and length of the defect have negligible influence on the tube strength. If the defect is in the deep position of the tube, the peak Mises stress decreases a little with the increase of the width of the defect, and increases a little with the increase of the length of the defect. But for all cases, the stress concentration becomes severe with the decrease of the width of the defect.

ACKNOWLEDGEMENTS

The financial supports provided by China National Science Foundation under Grant No. 51309236 is gratefully acknowledged. And we are grateful to Mr Kui Xu for his suggestion during this research.

References

1. J. B. Li, X. Hou, M.S Zheng, J. W. Zhu, *International Journal of Electrochemical Science*, 2 (2007) 607 – 617.
2. Y. N. Xue, S. J. Luo, M. Liu, R.Wang, *Corrosion Science and Protection Technology*, 25(2013) 24-29.
3. G. Q. Ren, Y. Shen, R. Wang, J. Wei, *Corrosion and Protection*, 36(2015) 245-250.
4. R. K. Liu, G. J. Yin, C. Y. Wei, *Corrosion Science and Protection Technology*, 25(2013) 451-455.
5. ASME B31G, America Society of Mechanic Engineering, USA (2009).
6. API-579-1/ASME FFS-1, American Petroleum Institute, USA (2009).
7. DNV-RP-F101, Det Norske Veritas, Norway (2004).
8. S.Z. Zhou, D. He and Z.P. Lu, *Oil Field Equipment*, 35 (2006) 19-22.
9. Y. Zhang, X. Peng and T. Huang, *Journal of Shenyang University of Technology*, 36 (2014) 526-531.
10. X.W. Hu, C.F. Zhou and M.L. Duan, *Petroleum Science*, 11 (2014) 139-146.
11. M. Y. Xia, Q. Q. Duan, X. B. Liu, H. Zhang, *Materials Science Forum*, 850(2016) 950-956.
12. J. Q. Shi, L. Jia, L. Deng, J. L. Hu, L. Wang, *Oil Field Equipment*, 45(2016) 10-16.
13. B. Fu, M.G. Kirkwood, Proceedings of the International Conference on Offshore Mechanics and Arctic Engineering, Copenhagen, Denmark, (1995) 165-184.
14. A.D. Batte, B. Fu and M.G. Kirkwood, Proceedings of International Conference on Offshore Mechanics and Arctic Engineering, Yokohama, Japan, (1997) 221-228.
15. J. B. Choi, B. K. Goo and J. C. Kim, *International Journal of Pressure Vessels and Piping*, 80 (2003) 121-128.
16. X.K. Zhu, B.N. Lei, *International Journal of Pressure Vessels and Piping*, 89 (2012) 85-97.
17. D.S. Cronin, Assessment of corrosion damage in pipeline, Department of Mechanic Engineering, University of Waterloo, Canada (2000).
18. Y.F. Chen, H. Zhang and J. Zhang, *Engineering Failure Analysis*, 47 (2015) 67-76.
19. B. Ma, J. Shuai, D. Liu and K Xu, *Engineering Failure Analysis*, 32 (2013) 209-219.

20. Y.F. Chen, X. Li and J. Zhou, *Journal of Ship Mechanics*, 13 (2009) 748-756.
21. J. Zhang, Z. Liang and C.J. Han, *International Journal of Electrochemical Science*, 10 (2015) 5036-5047.
22. M. X. Cui, F. J. He and M. Luo, *Acta Petrolei Sinica*, 01 (2003) 108-112.
23. ISO 10400, TR-2007. The International Organization for Standardization (2007).
24. API Specification 5CT, American Petroleum Institute, USA (2005).
25. ANSYS Release 12.1 Documentation, Ansys Inc, USA (2009).

© 2016 The Authors. Published by ESG (www.electrochemsci.org). This article is an open access article distributed under the terms and conditions of the Creative Commons Attribution license (<http://creativecommons.org/licenses/by/4.0/>).